An evening sector Ps 6 – omega band event

Martin Connors[1], Mikko Syrjäsuo[2], Eric Donovan[2], Mike Greffen[2], Brian Jackel[2], Trond Trondsen[2], Igor Voronkov[2], Robert L. McPherron[3], Christopher T. Russell[3], John Sigwarth[4], and Stephen B. Mende[5]

[1]Centre for Science, Athabasca University
[2]Physics and Astronomy, University of Calgary
[3]IGPP, UCLA
[4]University of Iowa
[5]Space Sciences Laboratory, University of California, Berkeley

Manuscript submitted to

Annales Geophysicae

Manuscript-No. ???

Annales Geophysicae, 0000, 0001–9, 2006
SRef-ID: 1432-0576/ag/2006-0000-0001

LOGO

An evening sector Ps 6 – omega band event

Martin Connors[1], Mikko Syrjäsuo[2], Eric Donovan[2], Mike Greffen[2], Brian Jackel[2], Trond Trondsen[2], Igor Voronkov[2], Robert L. McPherron[3], Christopher T. Russell[3], John Sigwarth[4], and Stephen B. Mende[5]

[1]Centre for Science, Athabasca University
[2]Physics and Astronomy, University of Calgary
[3]IGPP, UCLA
[4]University of Iowa
[5]Space Sciences Laboratory, University of California, Berkeley

Abstract. Ps 6 magnetic disturbances and associated optical forms known as omega bands are usually associated with the morning sector. Some evidence for similar phenomenology in the evening sector has been presented by Solovyev et al. (1999). We confirm and extend those results with high time resolution magnetic and imaging observations from Athabasca University Geophysical Observatory for an event that took place on July 27, 2003, along with conjugate hemisphere imaging from the Polar spacecraft. The observed signatures indicate sunward drift (westward in the evening sector). Magnetic perturbations feature negative Y and transitional Z indicating westward passage of poleward equivalent currents overhead. As has been suggested by Connors et al. (2003) to be often the case for morning sector Ps 6/omega bands, initiation of the evening sector event coincided with substorm onset. From optical and magnetic data we obtain consistent results for the drift rate of the forms, which changed during the event. An inner magnetospheric source is suggested, with triggering of the onset by an increase in solar wind speed.

1 Introduction

Ps 6 magnetic pulsations or disturbances are usually associated with the morning sector and are frequently accompanied by optical forms known as omega bands. The positive Y and transitional Z perturbations of the Ps 6 signal indicate localized regions of equatorward equivalent current in the auroral ionosphere, associated with the bright vortex–like forms of the omega bands. The currents (as inferred from magnetic perturbations) and the optical forms drift sunward (eastward in the morning sector) at speeds typical of bulk convection. In initial work by Saito (1974), their relation to substorms and to onset (Pi2) was realized. More recently they have usually been regarded as being associated with recovery phase (Amm et al, 2005). However, Connors et al. (2003) again stressed the association of morning sector Ps 6 signatures with substorm onset. (Solovyev et al., 1999) indicated that under certain conditions signatures similar to those of Ps 6, associated with optical forms similar to omega bands, could be found in the evening sector as well as the morning sector. Here we are able to confirm that result, and we further examine the relation to onset. In addition, we contrast satellite and ground imaging and use the latter in conjunction with magnetic inversion to obtain a drift rate of about 1 km/s for the evening forms.

Correspondence to: M. Connors (martinc@athabascau.ca)

We use magnetic data from numerous ground locations, ground imaging from Athabasca, space-based imaging by Polar in the conjugate hemisphere, and space plasma data from Cluster, Geotail and the geostationary GOES satellites. Cluster was situated in the morning sector near the plasma sheet, while Geotail was in the magnetosheath and is mainly of use in determining onset timing. The GOES 10 and 12 satellites were well placed bracketing the midnight sector. These positions are shown in Fig. 2. The Polar imaging sequence began very near the time of onset and Fig. 1 shows the aurora at the time of onset along with ground stations used and satellite footpoints. The auroral images from Polar were rectified from the southern hemisphere. Several points distibuted in the image field of view had their field lines traced to the northern hemisphere using the Tsyganenko model online at the Goddard Space Flight Center. Nonlinear optimization based on the Levenberg-Marquardt method (Press et al., 2002) was used to determine an optimal biquadratic transformation along field lines from geodetic positions in the southern hemisphere to the northern. A completely different approach to transformation based on PACE coordinates was also used (see below). The results were very similar between the two methods. The transformation was applied to all points in the image and the result gridded and plotted using the routines of Smith and Wessel (1990). Satellite footpoints were traced in a similar way and plotted as points, and geodetic positions of ground stations plotted directly.

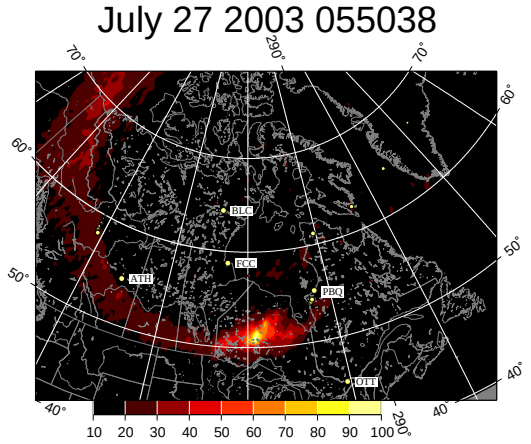

Fig. 1. Northern North America and Greenland showing auroral activity at the time on substorm onset 05:51UT on July 27, 2003, along with auroral observatories used in this study. The position of the Cluster footpoint is shown by four small yellow circles at hourly intervals starting in the NE (Greenland) at 5 UT and ending north of station PBQ at 8 UT. These circles grow with time. Similarly the GOES 10 (West) and GOES 12 (East) footpoints are shown as small clusters of growing yellow circles (for 0 to 8 UT). The GOES 12 footpoint is very near station PBQ. Auroral features are shown as projected from the southern hemisphere where they were imaged by the Polar spacecraft.

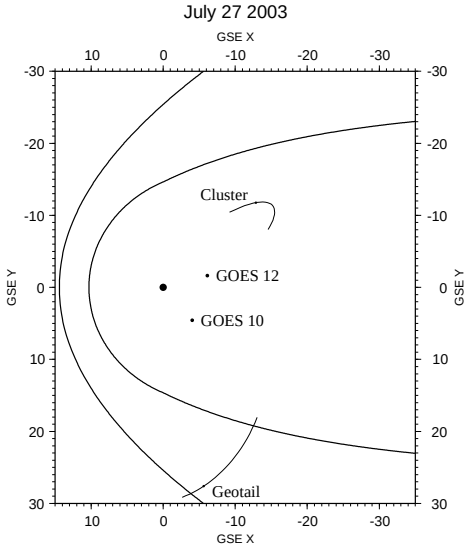

Fig. 2. Positions of the Cluster constellation, Geotail, GOES 10 and GOES 12 in GSE coordinates on July 27, 2000, with Earth at the origin. The position near 5:50 is indicated by a dot and motion throughout the day shown for Cluster and Geotail as a line. Nominal positions of the bow shock and magnetopause are shown as heavy lines.

2 Instrumentation and procedure

The Athabasca University Geophysical Observatory (AUGO) is a comprehensive facility for auroral studies located in the southern part of the western Canadian auroral zone. It provides a low noise and low light environment for geophysical measurements and has a high speed Ethernet fiber connection. AUGO has proved suitable for prototyping or testing equipment to be used during the THEMIS multi–spacecraft auroral mission. A UCLA "small" magnetometer and high time resolution monochrome all sky imager form a prototype ground based networked observatory similar to those now being installed to support the THEMIS mission (Donovan et al., 2006).

AUGO is located in central Alberta at geodetic coordinates 54.71835° N, 246.6871° E, corrected geomagnetic (2005) coordinates 62.04°, 306.46°, L–value 4.55, and with local magnetic midnight at 8:08 UT. It has operated a GPS–timed UCLA small magnetometer, taking 1 Hz local magnetic readings, since November 1998. One or more THEMIS white–light monochrome imagers have been in operation nearly continuously since May 2003. These consist of front optics designed and manufactured by Keo Consultants (R. Eather), with a commercial Starlight Xpress MX716 CCD camera as the detector for wideband (white light) imaging. The final image is 290×290 pixels with 16 bit digitization. They image the whole sky through a transparent dome at rates we have varied from one image per 5 seconds to one per 20 seconds, when the Sun is more than 10 below the horizon Connors et al. (2005). A station computer running Linux operates the imager autonomously using control software written by the University of Calgary. AUGO thus serves as an online prototype THEMIS ground station (although THEMIS magnetometers are an improved version and sample at 2 Hz). The current images were one second exposures taken every 20 seconds.

During 2003, the Polar spacecraft had perigee passes over the southern hemisphere, and thus good resolution imaging. For this particular event, good images from the Polar VIS camera Brittnacher et al. (1997) exist from the conjugate area. These are at a considerably lower cadence and resolution than it is possible to obtain from the ground. It is uncertain to what extent global space–based imaging will be available during the THEMIS mission. Due to the good spatial and temporal resolution possible from the ground, THEMIS has an extensive ground–based component Donovan et al. (2006). This event allows us to anticipate what one imaging spacecraft, in conjunction with THEMIS ground equipment, would be able to show about an auroral event. The

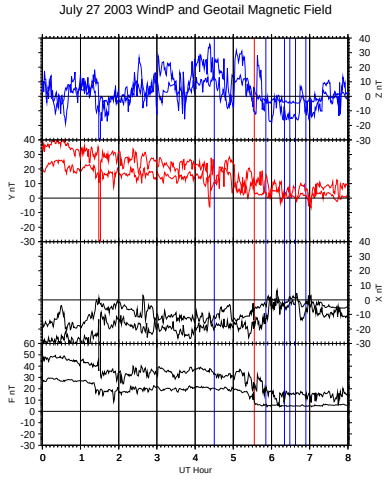

Fig. 3. Solar wind magnetic field propagated to the nose of the magnetosphere (heavy lines) and Geotail values (thin lines).

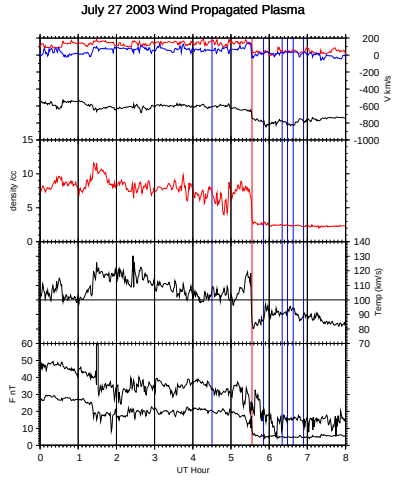

Fig. 4. Solar wind plasma properties propagated to the nose of the magnetosphere.

images from space are primarily useful to provide a global context, although they can also provide spectral information at wavelengths not able to be detected from the ground. If in fact no imaging spacecraft are operating during the THEMIS mission, global imaging context will be provided by a continental scale North American network of cameras similar to that described above. As we will show below, the high imaging cadence and level of detail seen in ground images also can be useful in determining detailed information about auroral morphology and motion. Early in the Polar mission, ground–Polar conjugate studies were done when the sunlit northern hemisphere was observed in the UV, while ground imaging was done from Antarctica in darkness (Frey et al., 1999). Mapping at those high latitudes required a magnetospheric model and deviations from conjugacy were noted. In our case the low L value allowed a simple procedure of converting image pixel locations into PACE coordinates (Baker and Wing, 1989), inverting the latitude, then reconverting to geodetic coordinates in the northern hemisphere. Images from the THEMIS ground camera were projected onto the sky and geometrically realigned for best comparison with the conjugated satellite images.

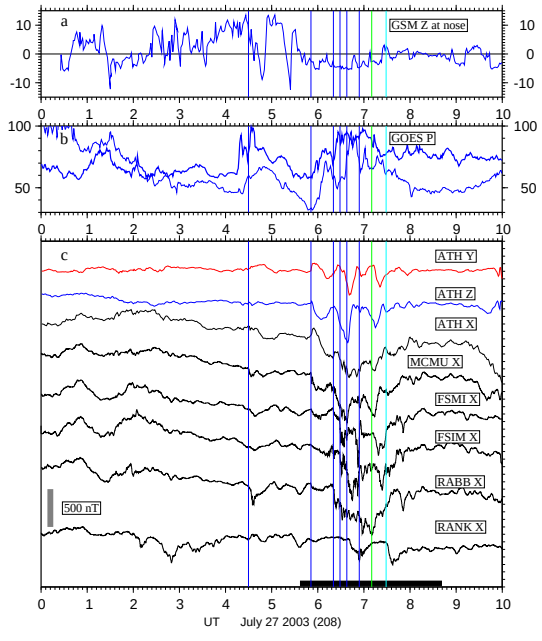

Fig. 5. (a) IMF B_Z, (b) GOES 10 (thin line) and 12 (thick line) poleward components, and (c) ground magnetic signatures.

3 Event overview

The Wind spacecraft was well situated to provide solar wind data for this event since it was near the Earth–Sun line and 140 RE in front of the Earth. Activity on July 26 was related to a sector boundary. It was an active day with dense although slow solar wind. Subsequently, fast–slow stream interaction dominated July 27, with major changes in all solar wind parameters in the period 05–06 UT as convected to the nose of the magnetosphere. The solar wind magnetic field, propagated (Weimer et al., 2003) for early parts of this day is shown in Fig. 3, along with values from Geotail, which was in the evening sector magnetosheath. The Geotail values are those of compressed solar wind and apart from absolute

value increases due to this compression, follow the propagated Wind values well. This indicates that the propagation was correct in its timing, but other than this the Geotail values are of little relevance to this study. Corresponding solar wind propagated plasma values are shown in Fig. 4. The discontinuity in these values at 05:33 UT is indicated by a red line. For comparison, Fig. 5 shows the IMF Z component as convected by simply applying a delay, based on the distance and the flow speed, to the nose of the Earth. The timing remains close to that from the propagation algorithm. The GOES 10 and 12 northward (P) component and selected ground magnetic field measurements are also shown. Up to 05:00 UT on July 27, the magnetic field was notable for its total field averaging over 20 nT. This declined to a very steady value near 5 nT, maintained after 05:30 UT. During the period of strong field, the Z component was mainly northward at about 10 nT. An isolated onset took place over North America at about 04:30 UT but is of no further interest here. At 05:49 UT on July 27, an onset took place over Canada and was well observed by our THEMIS camera and by the POLAR VIS imager in the conjugate region. This onset was not triggered by the major change in solar wind conditions as it followed them by at least 15 minutes. The onset timing was also confirmed by a clear onset of Pi2 pulsations in the CANOPUS array (not shown). At the time of and after this onset, evening sector omega bands were imaged and Ps 6 detected. Other onsets and poleward border intensifications (PBIs) followed.

The THEMIS camera was operated from 05:12:00 to 10:05:40 UT on July 27, 2003, with aurora visible in almost every frame. The POLAR VIS sequence began at 05:49:40 and continued to 08:42:19, with changing field of view in the southern hemisphere, including the conjugate region to Athabasca. Most exposures were of order 40 s, taken about every minute, but the imaging sequence included changes of wavelengths and of pointing direction/field of view. Thus, in the conjugate region iteself was imaged only about every five minutes. While this is useful for giving a global context, the motion of the omega bands is significant on this timescale, so that aliasing does not allow determination of their motion. This may be contrasted with the case of the Viking imager sequences, which did allow accurate tracking of the motion of individual omega bands Connors and Rostoker (1993). As will be the case with THEMIS, ground cameras are essential to determining motion of local auroral features like omega bands. In the case of THEMIS, the continental–scale imaging context will also be obtained by combining images from many cameras Donovan et al. (2006).

Fig. 7 detailed caption: (a) 061345 VIS Image Poleward Expansion. This image clearly shows the enhanced poleward border. Discrete auroras have moved poleward. The allsky view shows the diffuse aurora equatorward. Discrete aurora is to the north. (b) 062422 VIS Image Diffuse and Discrete. This image pair still shows the discrete auroras poleward of Athabasca and diffuse aurora to its south. Orientation is slightly different, with larger auroral region (top) more poleward as seen from the ground but in general conjugacy is excellent. (c) 063456 VIS Image Omega Bands. The appearance of the auroral oval has changed considerably, with poleward aligned forms, one of which is over Athabasca. At this time pulsating patches of aurora were observed from the ground as is typical on the morning sector when under the bright part of omega band. (d) 064553 VIS Image Gap of Omega Band. The omega bands have drifted westward (down) and Athabasca is now between bright forms. From the ground the bright forms west (top) and east (bottom) have different brightness than in the VIS but the geometry is consistent. (e) 065347 VIS Image Next Omega Band. The next omega band now covers Athabasca. Discrete auroras are located poleward. Pulsating aurora is overhead at Athabasca and the edges (top and bottom) of the torch of the omega band can be seen. Discrete auroras are to north (right) although there also appears to be cloud in that direction. (f) 070824 VIS Image Approaching Band. The next omega band is approaching Athabasca and is brightest to the northwest (above right) of it. Consistent with the satellite image, the approaching omega band is seen to the northwest while Athabasca is already under fainter pulsating auroras. Further, bright discrete auroras to the north have faded.

It is difficult to isolate a single cause of energization of the magnetosphere prior to this event. The density decreased by a factor of 3 while the speed increased from 600 to 800 km/s, resulting in a dynamic pressure drop by about a factor of two. The IMF was northward for most of the several preceding hours, with two large and sharp southward excursions and a gradual southward turning around the event time. However, higher than average solar wind speed has been inferred to assist in the development of Ps 6 in the morning sector, and likely played a role here also in favoring their appearance.

Triggering of the event appears to have been due to an increase in the absolute value of solar wind radial speed. This was inferred from plasma parameters propagated to the nose of the magnetosphere using the Weimer et al. (2003) technique.

4 Evening sector Ps 6

The growth phase appears to have started near the first major southward turning.

Growth phase appeared to start about 0500. Imaging and several other indicators show an onset at 05:50, with enhanced activity for a few minutes prior.

Other onsets took place at 0620, 0628, 0640, and 0654 UT. A small event at 0710 UT has been considered a pseudobreakup, and a high latitude event at 0728 UT a PBI. Subsequent Ps 6 pulses do not seem much affected by later onsets, an aspect noted by Connors and Rostoker (1993).

Fig. 5 shows onsets as blue lines. Growth phase is indicated at GOES10 by a decline in the poleward field starting 04:48 UT, near the first southward turning. The value at GOES 12 decreased after a clear sudden increase at dipolarization at 04:30, and was accompanied by an increase in the earthward component (not shown). These signatures of

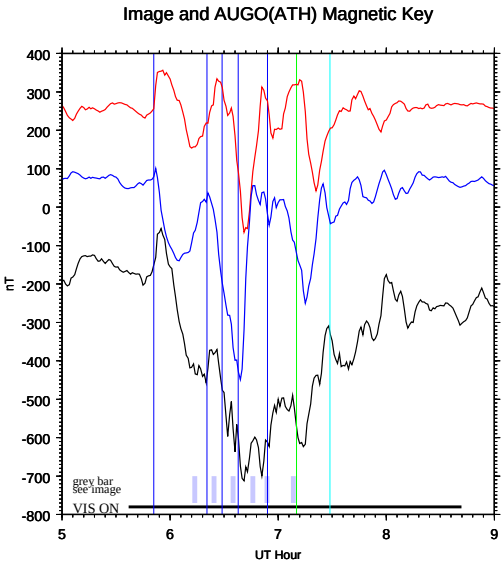

Fig. 6. Ground magnetic signatures from Athabasca. Vertical lines are events, short vertical bars are images shown below. Horizontal line is the period when VIS was taking images.

growth phase at geosynchronous orbit continued until the 05:49 onset.

5 Morning sector activity

The sparsity of ground stations in eastern Canada prevents a detailed study based on them. However, GOES 8 is nearly conjugate to the ground station at Poste de la Baleine, and the four Cluster II spacecraft were in the morning sector with numerous instruments including the magnetic field instrument Balogh et al. (2001) active. This gives the opportunity to study several aspects of the tail activity during this event, favoring the morning sector.

Cluster was at about 10 Re downtail and about 5 Re above the nominal (equatorial plane) position of the neutral sheet, in the morning sector with Y GSE also about 10 Re.

Precursory activity evident at Cluster included an event at 01:30, the first encounter of the edge of the plasma sheet on this day. There appears to be a strong field-aligned current in the boundary causing both By and Bz perturbations. This is probably the result of a substorm expansion since the edge of the sheet is nearly 6 Re above the equatorial plane. Since this is summer solstice, the neutral sheet is significantly above the equatorial plane. The Cluster spacecraft were just at the edge of the plasma sheet prior to 03:30. Apparently associated with the 04:30 onset, the 04:39 neutral sheet encounter has a bipolar signature in By that may be a flux rope nearly parallel to the X axis. Bz is monopolar as if a TCR had passed the spacecraft. Based on the curl approximation possible with

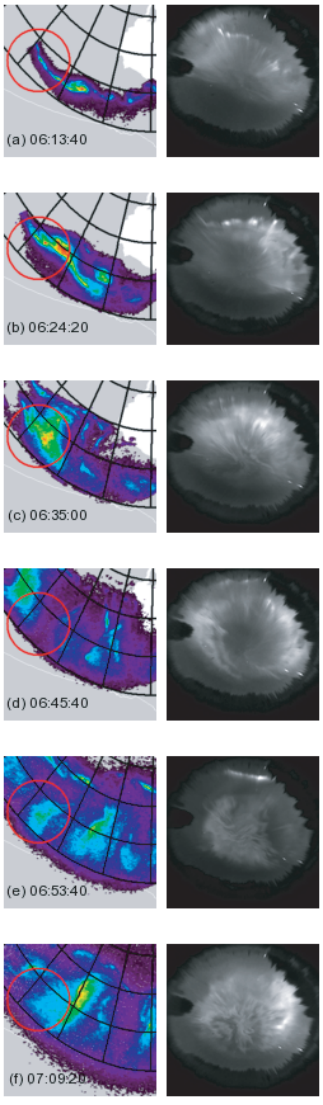

Fig. 7. VIS and corresponding THEMIS images. See text for detailed caption. (a) 061345 VIS Image Poleward Expansion. (b) 062422 VIS Image Diffuse and Discrete. (c) 063456 VIS Image Omega Bands. (d) 064553 VIS Image Gap of Omega Band. (e) 065347 VIS Image Next Omega Band. (f) 070824 VIS Image Approaching Band.

the four Cluster spacecraft, a nearly field-aligned current of over 20 nA/m^2 passed over the spacecraft at this time. This event is clearly a substorm signature as GOES-10 shows a dipolarization at 04:20 UT. Canopus also shows a weak bay signature.

The 05:25 neutral sheet encounter also looks like a field-aligned current effect caused by a substorm activation. However, the curl technique does not indicate any particularly strong currents at this time. This is early compared to Canopus data, but Cluster is around 0300 LT so is seeing some-

thing different than Canopus (a PBI).

Associated with the onset under study, the 05:53 signature is bipolar (+ then -) in Bz suggesting a TCR going tailward. This corresponds to the first onset and the GOES-10 dipolarization. However, it happened at 21 LT and Cluster spacecraft are at 03 LT - far away.

At 06:19 the plasma sheet must have thinned or tipped because Cluster are in the lobe.

6 Quantitative aspects of Ps 6/omega bands

The Ps 6 signal was observed in a limited area near Athabasca. The initiation of the Ps 6 signal at the 05:50 onset time is clear in Fig. 6 where the signal is prominent in Ym (red) and Z (blue). At onset the X component (black) initially rose, then declined. Four pulses of Ps 6 were seen as negative Ym: for two of these (0641 and 0720 UT) the transitional Z component is consistent with passage of a poleward equivalent current. There are also positive Ym excursions possibly indicating equatorward current preceding the passage of poleward current.

The Polar VIS data does not have a cadence allowing the drift velocity to be determined. Slow cadence was noted as a problem for the UVI instrument also by (Frey et al., 1999). Ground observations, both magnetometers and imagers at high cadence, allow this limitation to be overcome. Fig. 8 shows an ewogram, the analog of a keogram best suited for studying east–west motions such as are expected for omega bands Donovan et al. (2006). The ewogram was made by taking image slices across each of a sequence of images, perpendicular to the meridian and passing through the zenith, rotating these slim slices to the vertical, and stacking them side by side. As such, the ewogram shows east–west motions of intensity gradients in the auroral luminosity. This may be compared to a keogram, a standard method of showing intensity gradients in the north–south direction (usually in the meridian). The slices used in either technique may be of any width and may involve averaging. In this study the simplest method possible was used, which was to take a slice one pixel wide. Image values were extracted using the widely available pnm utilities, and the resulting matrix corresponding to the ewogram was gridded and plotted using the GMT tools (Smith and Wessel, 1990). Since we are focusing on morphology rather than data values, a nonlinear contrast stretch was applied (using linux tool xv) for optimum contrast. The resulting ewogram is shown with west at the top, east at the bottom.

In some optical systems the field is not very flat and geometric compensation must been done Connors et al. (2005). In the case of the THEMIS camera, we know from calibrations on similar optical systems that the field is rather flat. This means that pixels correspond well to angle on the sky. A simple calibration was done by finding the points corresponding to the horizons and using a linear transformation of pixel value to angle. From simple geometry using a flat Earth approximation, the zenith angle of a pixel along the

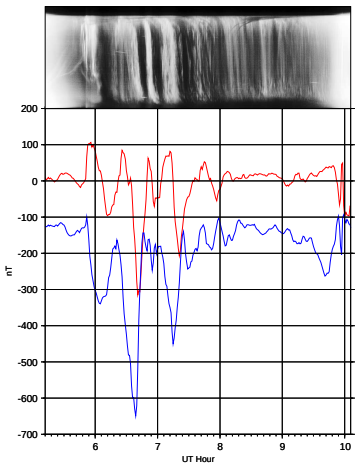

Fig. 8. Ewogram

east–west line is arctan(d/h) where h is the height at which the emission took place, and d is the distance away from the zenith. In drift at a constant speed, $d = v(t - -t_Z)$, where v is the speed of the drift, t the time, and t_Z the time at which the drifting form was at the zenith. We must also estimate the emission height h, since it cannot directly be determined with only one camera. In monochrome wideband imaging it is a fair assumption that most of the light is at the wavelength of the 557.7 nm forbidden oxygen auroral line. (Sigernes et al., 1996) used two meridian scanning photometers (MSPs) and the altitude of the maximum of 557.7 nm emission was found to vary between 125 and 160 km. (**?**) also used MSPs and found altitudes between 100 and 160 km depending on the solar depression angle.

Here, we initially assume that most of the emission comes from h=110 km, and revisit this assumption below. With this and the knowledge of t provided by the (GPS–timed) camera, the two parameters v and tZ characterize any drifting luminosity gradient. The latter parameter may be estimated from the ewogram directly. The v parameter characterizes the shape of the curve on the ewogram which corresponds to east–west motion. The locus of positions corresponding to a drifting form, as a function of time, is an arctan curve and is more steep the faster the drift. Such curves have been overplotted on a portion of the ewogram in Fig. 9. The v and t_Z parameters were varied and the resulting curves plotted over the ewogram until a good match between the edges of auroral forms and the tanh curve was obtained. In this way the parameters were estimated. In Fig. 9 the three curves correspond to drift at 1.0, 1.5, and 1.5 km/s, with a bright to dark transition drifting overhead at 6.7 UT, and a subsequent bright form drifting by between 6.84 and 6.915 UT.

The tanh–like curves persist through the whole event and

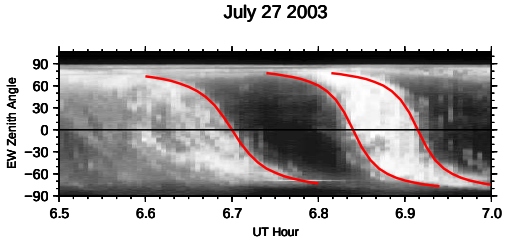

Fig. 9. Detail of ewogram overplotted with drift curves.

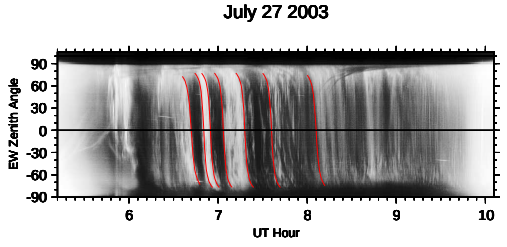

Fig. 10. Ewogram overplotted with drift curves for whole event.

are reasonably interpreted as corresponding to drift of brightness variations overhead. All are toward the west. It is more subtle to fit curves as described above when the contrast is not as great, but Fig. 10 shows such curves for the duration of the event. The deduced speeds are shown in the lower panel.

An alternate method of determining drift speeds relies on a simple magnetic model. It is well–known (Kawasaki and Rostoker, 1979) that the equivalent current system of Ps 6 in the morning sector corresponds to regions of equatorward flow of ionospheric current drifting eastward. The rise and decline of the YM (local magnetic eastward) component associated with peaks in the Ps 6 signal in the morning sector in the northern hemisphere occurs as the southward directed equivalent current passes over the station, with the maximum being when it is overhead. The Z component is transitional from negative to positive: this corresponds to upward perturbations when the southward directed equivalent current is west of the observing station and to downward perturbations when it has drifted to the east. In this model the X_M (local magnetic northward) component does not experience any perturbations. It is clear from examining Fig. 6 that the Y_M perturbations for this evening sector event are reversed from those of morning sector Ps 6, with primarily negative perturbations, corresponding to passage overhead of poleward–flowing equivalent current regions. The transitional Z is that associated with such currents drifting westward. We do not in this study attempt to distinguish between whether the true current systems responsible for Ps 6 involve field–aligned currents to complete the equivalent current loop (Kawasaki and Rostoker, 1979) or mainly have currents localized in the ionosphere and strong conductivity gradients (Amm et al, 2005). We simply state that the observed perturbations can be reproduced to first order by the westward drift of a narrow region of poleward current at ionospheric height.

Using a modeling routine which can return those parameters of a forward model which best reproduce ground observations, one can determine the geometric parameters and electric current in a three–dimensional current system (Connors , 1998; Connors and Rostoker, 2002). Normally such a procedure is done with data from many ground stations. In this case, the scale length of the current systems is small and the Ps 6 events perturbations were detected with any strength only at the one station of Athabasca. Since the Ps 6 perturbations were significant only in two components (Y_M and Z), there are only two data points at each time upon which to base magnetic optimization. The Ps 6 X_M being zero is implicitly used since the forward model will use only a poleward current which cannot produce nonzero X_M perturbations. In principle, the free parameters of the poleward current system are its longitude and the strength of the current, which could be determined with two data points. In practice, distinguishing between a large current far away and a weaker one nearby is difficult, especially in the presence of noise. Thus it was determined that the peak currents involved in producing the Ps 6 signal, based on the extema of the YM component, were about 400 kA. Over the local region, this figure is not expected to change much as the forms drift, thus the current was constrained to this value. Only the longitude of the current was determined by optimization based on two magnetic data inputs at any time. We note in passing that the optimization routine uses as its basic element a region of current flow and normally has field–aligned currents.

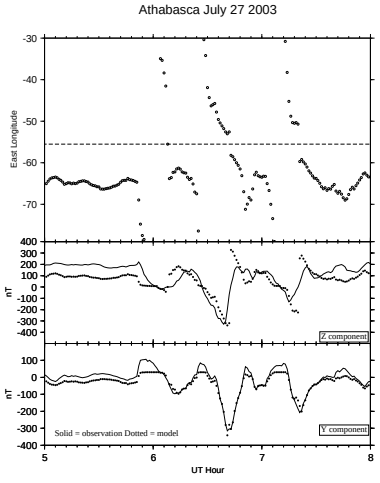

Fig. 11. Magnetic inversion results. Top panel is longitude of the equivalent north–south line current. Middle panel is the model results for the Z component (dots) compared to the observations (solid). Bottom panels shows the same comparison for the Y component.

It is however, possible to constrain parameters in relation to each other (Connors , 1998). In this case the region was constrained in such a way that it corresponded to a filamentary current, and that the field–aligned currents were far from the station. The results presented are thus those for a north–south aligned filamentary current, at ionospheric height taken to be 110 km, of 400 kA strength. Earth induction (Kisabeth, 1979) is included, so that 400 kA is close to the true current strength.

Fig. 11 shows the longitude of such a current system over time. At the times near approximately 6.7 and 7.3 UT, the derived longitude changed systematically, with a progression to more negative east longitudes indicating a westward motion of the current system. At these times the model perturbations closely matched those of the two largest Ps 6 perturbations in both the Y_M and Z components. For purposes of modeling, the Y_M component was adjusted to have near–zero perturbations at non–perturbed times, while the Z component was adjusted to be near zero at the extrema of Y_M. This allows the simple filamentary current model to represent the perturbations well. We do note, however, that a jump in longitude took place near the time of current passage over the station (dashed line), and that Z perturbations were not well reproduced immediately after passage. These problems can be attributed to the current magnitude being slightly incorrect, and to a more complex real current system with some asymmetries. Nevertheless, the general agreement of modeling results to observations suggests that the essentials of the current system have been reproduced well enough for our simple purpose. By using the times when the longitudes were about –45° and –65°, it can be concluded that the speed of drift during the first Ps 6 perturbation was 1.03 km/s, while that during the second one was 1.46 km/s. The first perturbation corresponds to that at 6.7 UT examined in detail in Fig. 9 and for which the optical drift speed was calculated at 1.0 km/s. The second perturbation occurred after the drift speed had increased to 1.5 km/s as determined from the ewograms. Although it is possible to do this for only two Ps 6 pulses, there is a good degree of consistency between the optical and magnetic methods of obtaining drift speeds. This shows that the magnetic inversion technique can be used to determine drift speeds. Since the optical inversion from one camera is based on an assumption of an emission height whereas the magnetic technique is not very sensitive to the height of the currents, the agreement of the two independent techniques also supports the original estimate that the optical emissions did arise from 110 km altitude.

7 Conclusions

We verify that pulsations similar to morning sector Ps 6 also occur in the evening sector. Similarly, they are associated with forms resembling omega bands both on the large scale as viewed by satellite, and on the small scale as viewed by an allsky camera. Similar to morning sector omega bands and consistent with the general large–scale plasma convection, the omega bands drift sunward, which is westward in this local time sector.

The magnetic signal is also associated with westward drift and may be due to poleward equivalent ionospheric currents. The westward drift directly observed for the omega bands and best deduced from an ewogram was consistent with that which could be derived from magnetic modeling for two prominent Ps 6 perturbations. This drift was in the range of 1.0 to 1.5 km/s which has been deduced before (e.g. Connors and Rostoker, 1993), and is near the convection speed during a disturbed time (Amm, 1996).

The initiation of the Ps 6 train was at onset time as has been noted for the morning sector (Connors et al., 2003). However, subsequent onsets did not affect the timing of Ps 6 pulses as has been noted for the morning sector (Connors and Rostoker, 1993).

Despite the high activity level, excellent conjugacy was inferred between the ground in the northern hemisphere and satellite imaging in the southern hemisphere. This implies that tracing to magnetospheric source regions should be accurate. Since the L value at Athabasca is only about 4.5, the Ps 6 and omega bands associate to the inner magnetosphere, as previously noted for many morning sector Ps 6 events (**?**). The global imaging shown here places the omega bands near the equatorward boundary of the auroral oval, not at the poleward boundary as has often been posited for morning sector omega bands (Amm et al, 2005, e.g.). Connors et al. (2003) presented evidence from magnetic profiles that morning sec-

tor Ps 6 could be located at either the equatorward or poleward boundary.

At least in the case of the first pulsation of the sequence presented here, some relation to the westward traveling surge (WTS) is possible. As discussed by Opgenoorth et al. (1983), a surge–like form in the morning sector had been proposed as responsible for morning–sector Ps 6. The relation to onset noted here, and for morning sector forms by Connors et al. (2003) makes such an identification plausible.

These results suggest that Kelvin–Helmholtz instablilities, the likely cause of the morning sector features, can also excite waves in the evening sector under appropriate circumstances.

Acknowledgements. We wish to acknowledge the following PIs who provided data to NASA Goddard Space Flight Centers CDAWeb: K. Ogilvie, MIT (Wind SWE), R. Lepping, NASA/GSFC (Wind MFI), and Howard Singer, NOAA/SEC (GOES MFI). Cluster data was used courtesy of the Cluster FGM Team. We thank James Weygand for Wind data propagated to Earth with the Weimer technique. We also acknowledge GSFCs SSC and IGRF/Tsyganenko tracing facilities. The CANOPUS instrument array, constructed, maintained and operated by the Canadian Space Agency, provided data for this study and we were assisted by Fokke Creuzberg. Further magnetic data examined included that from NRCan, Alaska (PI John Olson), and USGS through INTERMAGNET. This work has been funded by NSERC and the Canada Research Chairs program. Athabasca University Geophysical Observatory was established using funding from the Canada Foundation for Innovation and Alberta Innovation.

References

Amm, O.: Improved electrodynamic modeling of an omega band and analysis of its current system, J. Geophys. Res. 101, 2677—-2684, 1996

Amm, O., Aksnes, A., Stadsnes, J., Østgaard, N., Vondrak, R. R., Germany, G. A., Lu, G., Viljanen, A.: Mesoscale ionospheric dynamics of omega bands determined from ground–based electromagnetic and satellite optical observations, Annales Geophys. 23, 325—-342, 2005

Baker, K. B. and Wing, S.: A new magnetic coordinate system for conjugate studies at high latitudes, J. Geophys. Res. 94, 9139—-9143, 1989

Balogh, A., Carr, C.M., Acua, M–H., Dunlop, M.W., Beek, T.J., Brown, P., Fornacon, K.–H., Georgescu, E., Glassmeier, K.–H., Harris, J.P., Musmann, G., Oddy, T.M. and Schwingenschuh, K.: The Cluster magnetic field investigation: Overview of in–flight performance and initial results, Ann. Geophys., 19, 1207—-1217, 2001

Brittnacher, M., Spann, J., Parks, G., and Germany, G.: Auroral observations by the polar Ultraviolet Imager (UVI) Adv. Space Res. 20, 1037—-1042, 1997

Connors, M.: Auroral Current Systems Studied Using Automated Forward Modelling, Ph.D. Thesis, Department of Physics, University of Alberta, 410 pp., 1998

Connors, M., and Rostoker, G.: A Substorm Sequence Studied with Automated Forward Modeling, in Sixth International Conference on Substorms (ISBN 0–9711740–3–2), R. Winglee, ed., University of Washington Press, Seattle, 490—-495, 2002

Connors, M., Rostoker, G., Sofko, G., McPherron, R. L., and Henderson, M.: Ps 6 Disturbances: Relation to Substorms and the Auroral Oval, Ann. Geophys. 21, 493—-508, 2003

Connors, M., Syrjäsuo, M., Brown, P., and Donovan, E.: Meteor and Aurora Detection using Modern Video Technologies, J. Royal Astr. Soc. Canada 99, 14—-22, 2005

Connors, M., and Rostoker, G.: Source Mechanisms for Morning Auroral Features, Geophys. Research Letters 20, 1535—-1538, 1993

Deehr et al. (Annales Geophysicae, 2005, 23: 1–8)

Donovan, E., Mende, S., Jackel, B., Frey, H., Syrjsuo, M., Voronkov, I., Trondsen, T., Peticolas, L., Angelopoulos, V., Harris, S., Greffen, M., and Connors M.: The THEMIS All–Sky Imaging Array – System Design and Initial Results from the Prototype Imager, in press, Journal of Atmospheric and Solar–Terrestrial Physics, 2006

Frey, H. U., Mende, S. B., Vo, H. B., Brittnacher, M., and Parks, G. K.: Conjugate Observations of Optical Aurora with POLAR satellite and ground–based cameras, Adv. Space Res. 23, 1647–1653, 1999

Kawasaki, K., and Rostoker, G.: Perturbation Magnetic Fields and Current Systems Associated with Eastward Drifting Auroral Structures, J. Geophys. Res. 84, 1464—-1480, 1979

Kisabeth, J. L.: On Calculating Magnetic and Vector Potential Fields due to Large–Scale Magnetospheric Current Systems and Induced Currents in an Infinitely Conducting Earth, in Quantitative Modeling of Magnetospheric Processes, edited by W. P. Olson, American Geophysical Union, Washington, pp. 473—-498, 1979

Opgenoorth, H. J., Oksman, J., Kaila, K. U., Nielsen, E., and Baumjohann, W.: Characteristics of Eastward Drifting Omega Bands in the Morning Sector of the Auroral Oval, J. Geophys. Res. 88, 9171—-9185, 1983

Press, W. H., Teukolsky, S. A., Vetterling, W. T, and Flannery, B. P.: Numerical Recipes in C++, Cambridge, New York, 2002

Pulkkinen, T. I., Pellinen, R. J., Koskinen, H. E. J., Opgenoorth, H. J., Murphree, J. S., Petrov, V., Zaitzev, A., and Friis–Christensen, E.: Auroral Signatures of Substorm Recovery Phase: A Case Study, in Magnetospheric Substorms, J. R. Kan, T. A. Potemra, S. Kokobun, and T. Iijima, Eds., American Geophysical Union, Washington, 333—-339, 1991

Saito, T.: Examination of the Models for the Substorm–Associated Magnetic Pulsation, Ps6, The Science Reports of the Tôhoku University Ser. 5, Geophysics, Vol. 22 No. 2, 35—-59, 1974

Sigernes et al. (GRL vol 23, no 14, pages 1889—-1892, 1996)

Smith, W. H. F., and Wessel, P.: Gridding with a Continuous Curvature Surface in Tension, Geophysics, 55, 293—-305, 1990

Solovyev, S. I., Baishev, D. G., Barkova, E. S., Engebretson, M. J., Posch, J. L., Hughes, W. J., Yumoto, K., and Pilipenko, V. A.: Structure of Disturbances in the Dayside and Nightside Ionosphere during Periods of Negative Interplanetary Magnetic Field BZ, J. Geophys. Res. 104, 28019—-28039, 1999

Weimer,D.R., Ober,D.M., Maynard,N.C., Collier,M.R., McComas, D. J., Ness,N.F., Smith,C.W., and Watermann,J. 2003, Predicting interplanetary magnetic field (IMF) propagation delay times using the minimum variance technique, J. Geophys. Res. 108, SMP 16–1, DOI 10.1029/2002JA009405, 2003